Progress of Theoretical Physics, Vol. 49, No. 3, March 1973

X-Ray Emission from White Dwarfs in Close Binary Systems

Reiun HŌSHI

Department of Physics, Rikkyo University
Nishi-Ikebukuro, Tokyo

(Received September 30, 1972)

The generation of X-ray sources in close binary systems is studied. It is proposed that one of the stars is a white dwarf and it is accreting material from its companion. The entire treatment applies to the spherically symmetric and the stationary case. The model of this type accounts qualitatively for the observed nature of SCO X-1.

§ 1. Introduction

Recently, observational knowledge of X-ray sources has been accumulated extensively, of which the most interesting fact is the variability of X-ray sources with various time scales. It seems that the variability is the common property inherent to X-ray sources.

SCO X-1 is an X-ray source which has been observed in great details. The temperature of hot plasma and the emission measure, which are determinable from the observed intensities in several energy ranges, show different values depending on the time at which observations are made. A remarkable correlation will be seen when observational values are plotted in the temperature-emission measure diagram.[1)]

From simultaneous observations of the X-ray intensity and the optical blue-magnitude of SCO X-1, one can also find a correlation between the temperature and the B-magnitude,[1)] though not so remarkable as in the former. It seems that these correlations as well as other observational evidences such as the excess of high-energy X-ray intensity, radio emissions, etc., give an important clue for the study of physical entity for X-ray sources.

One of the most exciting discovery in X-ray source is the recently reported evidence[2)] that the pulsating source Cen X-3 is a member of an eclipsing binary system. Analysis of Cen X-3 gives the upper limit of the mass of the X-ray source, which has been estimated to be about $0.5\,M_{\odot}$.[3)] This mass is typical for the white dwarf, though a possibility of a neutron star cannot be excluded. However, the formation of a neutron star through a supernova explosion may be incompatible with the observed circular orbit of Cen X-3.

We were motived from this fact to consider that some of X-ray sources may be explained by accretion of matter on to a white dwarf. The motion of infall-

ing material becomes soon supersonic on account of the gravitational field of the white dwarf. As was pointed out by Sakashita,[4] a standing shock wave appears near the surface of the white dwarf. Through the shock, most of the kinetic energy of infalling material convert to the thermal energy of the gas. X-rays are emitted from the narrow zone between the shock discontinuity and the surface of the star. The mean temperature and the size of this emission region will be approximately determined in § 2.

In § 3 the mean temperature, the corresponding emission measure and the X-ray luminosity are numerically calculated for white dwarfs of mass $0.5\,M_\odot$, $0.6\,M_\odot$ and $0.7\,M_\odot$, respectively.

As is expected, the model thus calculated accounts qualitatively for the observed nature mentioned above. Details of the comparison will be studied in § 4.

§ 2. A binary model of X-ray source

As for the center of gravitational attraction, we consider a white dwarf with the mass M and its radius R. It is assumed that the white dwarf acts as a sink for any infalling material from its companion, but the consequent increase in mass is neglected. The motion of infalling material is assumed to be spherically symmetric and the flow to be stationary. In addition, we assume the gas to be perfect and to have constant specific heats with ratio γ.

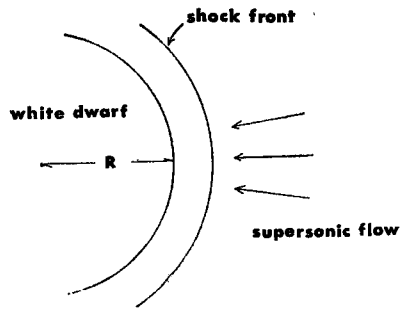

Fig. 1. Schematic diagram of mass-accretion by a white dwarf.

On account of the gravitational field of the white dwarf, the flow is expected to be highly supersonic in the vicinity of the star. Consequently, a spherical standing shock wave appears in front of the surface of the star, as is shown schematically in Fig. 1.

In the following, the physical nature of the flow in these situations will be studied under reasonable approximations.

1) *Infalling flow*

If we assume the motion to be adiabatic for infalling flow toward the shock front, it can be represented by Bernoulli's equation[5]

$$\frac{1}{2}v^2+\frac{1}{\gamma-1}c_s^2-\frac{GM}{r}=\text{const}, \tag{1}$$

where c_s is the local sound velocity and M the mass of the white dwarf. The constant in Eq. (1) is determined from the boundary conditions. As is usual in a stationary flow under gravitational attraction, the constant can approximately be put to zero, as far as the flow in the vicinity of the star is concerned.[4]

Furthermore, in the limit of a supersonic flow, Eq. (1) can be written simply as

$$\frac{1}{2}v^2=\frac{GM}{r}. \tag{2}$$

2) *Shock discontinuity*

Let the velocities before and behind the shock discontinuity be v_1 and v_2 in the coordinate system co-moving with the shock front. In the following, subscripts 1 and 2 describe the quantities before and behind the shock discontinuity, respectively. The Rankine-Hugoniot relation[6] gives

$$v_1=\frac{\gamma+1}{4}U+\sqrt{\frac{(\gamma+1)^2}{16}U^2+c_{s,1}^2}, \tag{3}$$

where

$$U=v_1-v_2. \tag{4}$$

In the limit of a strong shock, $v_1/c_{s,1}\gg 1$, we have

$$v_1=\frac{\gamma+1}{2}U=\frac{\gamma+1}{2}(v_1-v_2). \tag{5}$$

For the spherical standing shock which will appear around the central star, the velocity behind the shock is given by

$$v_2=\frac{\gamma-1}{\gamma+1}v_1, \tag{6}$$

where v_1 is given by Eq. (2), because the shock front is at rest with respect to the central star. Also, in the limit of a strong shock, the jump of the density and the temperature are given by[6]

$$\frac{\rho_2}{\rho_1}=\frac{\gamma+1}{\gamma-1},\quad \frac{T_2}{T_1}=\frac{2\gamma(\gamma-1)}{(\gamma+1)^2}\left(\frac{v_1}{c_{s,1}}\right)^2. \tag{7}$$

From Eqs. (2), (6) and (7), the velocity and the temperature behind the shock are written as

$$v_2=\frac{\gamma-1}{\gamma+1}\sqrt{\frac{2GM}{r_1}}, \tag{8}$$

$$T_2=\frac{2(\gamma-1)}{(\gamma+1)^2}\frac{\mu H}{k}\frac{2GM}{r_1}, \tag{9}$$

where μ and H are the mean molecular weight for accreting material and the hydrogen mass, respectively.

Suppose that the shock front is produced close to the star's surface (this is the case as will be discussed later), then the distance r_1 can be replaced by the radius of the star R. In Table I, the velocity v_1 and the temperature T_2 are tabulated for three different masses of white dwarfs. Here, g describes the

Table I. Physical data for white dwarfs accompanying the accretion of material.

$M/M_\odot$	0.5	0.6	0.7
$\log R$ (cm)	8.99	8.94	8.90
$\log g$ (cm/sec^2)	7.85	8.02	8.18
$\log v_1$ (cm/sec)	8.57	8.63	8.69
$\log T_2$ (°K)	8.28	8.41	8.52

gravity at the surface of the star. White dwarfs are assumed to be complete degenerate configurations. The mass-radius relation has been interpolated from the Table of Chandrasekhar.[7]

3) *Emission region*

Most of X-rays are emitted in the region enclosed by the shock front and the surface of the star. Hereafter, this region will be called the emission region. The emission region is described by the equation of continuity, momentum balance and conservation of energy as

$$r^2\rho v_r = \text{const}, \tag{10}$$

$$v_r\frac{dv_r}{dr}+\frac{1}{\rho}\frac{dP}{dr}+\frac{GM}{r^2}=0\,, \tag{11}$$

$$\rho v_r\frac{d\varepsilon}{dr}+\frac{P}{r^2}\frac{d}{dr}(r^2v_r)+\varepsilon_{\rm ff}\rho=0\,, \tag{12}$$

where ε and $\varepsilon_{\rm ff}$ are the specific internal energy and the emission rate of energy per unit mass due to the free-free process, respectively. In deriving Eq. (12), it is assumed that the emission region is transparent for emitted radiations.

Now, we assume the thickness of the emission region x to be much smaller than the stellar radius, $x\ll R$. The pressure in the emission region must increase toward the center, $dP/dr<0$, while the temperature must decrease, $dT/dr>0$. The flow velocity v_r in the above equations has negative value since we are interested in the case of accretion. Denoting its magnitude as v, Eqs. (11) and (12) are approximately expressed as

$$v\frac{v}{x}-\frac{1}{\rho}\frac{P}{x}+\frac{GM}{R^2}=0\,, \tag{13}$$

$$-v\frac{\varepsilon}{x}-\frac{P}{\rho}\frac{v}{x}+\varepsilon_{\rm ff}=0\,. \tag{14}$$

The emission rate of energy is given by[8]

$$\varepsilon_{\rm ff}=\varepsilon_0\rho T^{1/2}\quad(\text{ergs/gm sec}), \tag{15}$$

where

$$\varepsilon_0=4\sqrt{\frac{\pi}{2}}\left(\frac{8e^6}{3\pi c^2 m\hbar}\right)\left(\frac{k}{mc^2}\right)^{1/2}\frac{1}{\mu_e}\sum_i\frac{Z_i^2}{\mu_i}\bar{G}(T,Z_i)\,. \tag{16}$$

The mean molecular weights for electrons and i-th species of ions are described by μ_e and μ_i, respectively. For simplicity the integrated gaunt factor $\bar{G}$ is approximated by $2\sqrt{3}/\pi$.[9] The specific internal energy can simply be written as

$$\varepsilon=\frac{1}{\gamma-1}\frac{k}{\mu H}T. \tag{17}$$

By means of the above equations, the thickness of the emission region is given by

$$x=(c_s^2/\gamma-v^2)/g, \quad g=\frac{GM}{R^2}, \tag{18}$$

and for the temperature we have

$$T=\left\{\frac{\mu H}{k}\frac{\gamma-1}{\gamma}\varepsilon_0 A\frac{x}{v^2}\right\}^2, \tag{19}$$

where the accretion rate per unit area is denoted by

$$A\equiv\rho v=\frac{1}{4\pi R^2}\frac{d\mathcal{M}}{dt}. \tag{20}$$

As is clearly understood from Eq. (14), the temperature determined from Eq. (19) has a meaning that the total amount of energy emitted from a given mass element of infalling material, $\varepsilon_{\rm ff}t=\varepsilon_{\rm ff}(x/v)$, is just equal to the enthalpy of this mass element, $\varepsilon+P/\rho$. Then, it can be interpreted as the effective temperature of the emission region, and it is denoted by $\bar{T}$. It is to be noticed that the effective temperature depends on the thickness x. It is determined from the relation that the pressure must balance with both the gravity and inertia force, i.e., $P=\rho gx+\rho v^2$, as given by Eq. (18).

Inserting Eq. (18) into (19), we obtain the quadratic equation for the temperature, which can be solved when the accretion rate A and the mean velocity v are specified. Since the mean flow velocity must asymptotically tend to zero at the base of the emission region, it is taken simply as

$$v^2=\tfrac{1}{2}v_2^2. \tag{21}$$

The total X-ray luminosity can be obtained from the generalized Bernoulli's equation:

$$L_{\rm ff}=\left\{\frac{1}{2}v_1^2+\frac{\gamma}{\gamma-1}\frac{k}{\mu H}(T_1-T_s)\right\}\frac{d\mathcal{M}}{dt}, \tag{22}$$

where T_s is the temperature at the base of the emission region. The second term in the large bracket can be neglected when $T_2\gg|T_1-T_s|$.

§ 3. Result of numerical calculation

Numerical calculation has been done for three different masses of white dwarfs, $0.5\,M_\odot$, $0.6\,M_\odot$ and $0.7\,M_\odot$, respectively.

The chemical composition of accreting material is assumed to be

$$X=0.7, \quad Y=0.3, \tag{23}$$

where X and Y are the fraction of hydrogen and helium, by weight, respectively.

A convenient method is to specify an effective temperature, and then, determine the corresponding thickness and accretion rate from Eqs. (18) and (19).

Results are shown in Table II where numerical values are listed as a function of the accretion rate $d\mathcal{M}/dt$. The density behind the shock discontinuity is denoted by ρ_2. In the last column the emission measure is listed, which is calculated along

$$\overline{n_e^2 V} = L_{\rm ff} / \{\varepsilon_0 (\mu_e H)^2 \overline{T}^{1/2}\}. \tag{24}$$

Table II(a). Characteristics of the emission region for a white dwarf of $M=0.5M_\odot$.

$d\mathcal{M}/dt(10^{-7}M_\odot/\mathrm{yr})$	$\log x$ (cm)	$\log \overline{T}$ (°K)	$\log \rho_2$ (gm/cm^3)	$\log L_{\rm ff}$ (ergs/sec)	$\log \overline{n_e^2 V}$ (cm^{-3})
46.8	6.26	7.52	−6.57	37.30	60.70
14.5	6.78	7.54	−7.08	36.80	60.18
5.25	7.26	7.62	−7.52	36.35	59.70
2.91	7.56	7.71	−7.78	36.10	59.40
1.95	7.78	7.80	−7.95	35.93	59.18
1.46	7.96	7.90	−8.08	35.80	59.00
1.19	8.08	7.98	−8.16	35.71	58.88
0.92	8.26	8.10	−8.28	35.60	58.70
0.77	8.39	8.20	−8.35	35.52	58.58

Table II(b). Characteristics of the emission region for a white dwarf of $M=0.6M_\odot$.

$d\mathcal{M}/dt(10^{-7}M_\odot/\mathrm{yr})$	$\log x$	$\log \overline{T}$	$\log \rho_2$	$\log L_{\rm ff}$	$\log \overline{n_e^2 V}$
64.9	6.21	7.64	−6.40	37.57	60.91
20.1	6.74	7.67	−6.90	37.07	60.38
7.29	7.21	7.74	−7.35	36.62	59.91
4.05	7.51	7.83	−7.60	36.37	59.61
2.71	7.74	7.93	−7.78	36.19	59.38
2.02	7.91	8.03	−7.90	36.07	59.21
1.66	8.04	8.11	−7.99	35.98	59.08
1.28	8.21	8.23	−8.10	35.87	58.91

Table II(c). Characteristics of the emission region for a white dwarf of $M=0.7M_\odot$.

$d\mathcal{M}/dt(10^{-7}M_\odot/\mathrm{yr})$	$\log x$	$\log \overline{T}$	$\log \rho_2$	$\log L_{\rm ff}$	$\log \overline{n_e^2 V}$
87.1	6.17	7.75	−6.24	37.81	61.09
26.7	6.69	7.78	−6.75	37.30	60.56
9.68	7.17	7.86	−7.19	36.86	60.09
5.37	7.47	7.95	−7.40	36.60	59.79
3.60	7.69	8.04	−7.62	36.43	59.56
2.69	7.87	8.14	−7.75	36.30	59.39
2.20	7.99	8.22	−7.83	36.22	59.26
1.69	8.17	8.34	−7.95	36.10	59.09

From Table II one can see that both the thickness x and the effective temperature $\bar{T}$ decrease as the accretion rate is increased. The emission region becomes dense in the phase of a large accretion rate. Correspondingly, more energy is emitted because $\varepsilon_{ff} \propto \rho T^{1/2}$. The emission region is then cooled and the temperature is lowered. As a result, the emission region is confined in a more compressed state in order to recover a necessary pressure.

Finally, one can see from Table II that the approximation $x \ll R$ can be fully satisfied except for higher-temperature phases.

§ 4. Physical property of model

In this section we will discuss some properties of the model in comparison with the observational knowledge of X-ray source. However, since the numerical result thus far obtained is very approximate, we will not discuss its detailed comparison but discuss only its overall nature. In the following, as an example, the result for the case of mass accretion on to 0.5 $M_\odot$ white dwarf will be compared with the observations of SCO X-1.

1) *Emission measure*

The emission measure was calculated as listed in the last column of Table II(a). On the other hand, $\overline{n_e^2 V}/4\pi d^2$ (where d is the distance to the X-ray source) was determined from X-ray observations of SCO X-1.[1] Comparison of the both figures enables us to estimate the distance to SCO X-1. Theoretical values $\overline{n_e^2 V}/4\pi d^2$ are shown in Table III, where the distance is assumed to be $d=150$ pc so as to obtain a reasonable fitting to the observations. These are illustrated in Fig. 2 by a solid curve, as well as the observations denoted by rhombic error boxes.

The spread of observational values in this diagram can be understood as follows: In our model, both the emission measure and the effective temperature have to be determined depending on the rate of accretion of infalling material. The upper half of Fig. 2 shows the corresponding accretion rate, from which one can see that accretion rates are different in each observation.

Table III. The effective temperature and the emission measure as a function of the accretion rate ($M=0.5M_\odot$, $d=150$ pc).

$d\mathcal{M}/dt$ ($10^{-7}M_\odot$/yr)	$k\bar{T}$ (KeV)	$\overline{n_e^2 V}/4\pi d^2$ (10^{16} cm^{-5})
5.25	3.56	18.7
2.91	4.38	9.33
1.95	5.47	5.61
1.46	6.84	3.73
1.19	8.21	2.80
0.92	11.0	1.87
0.77	13.7	1.40

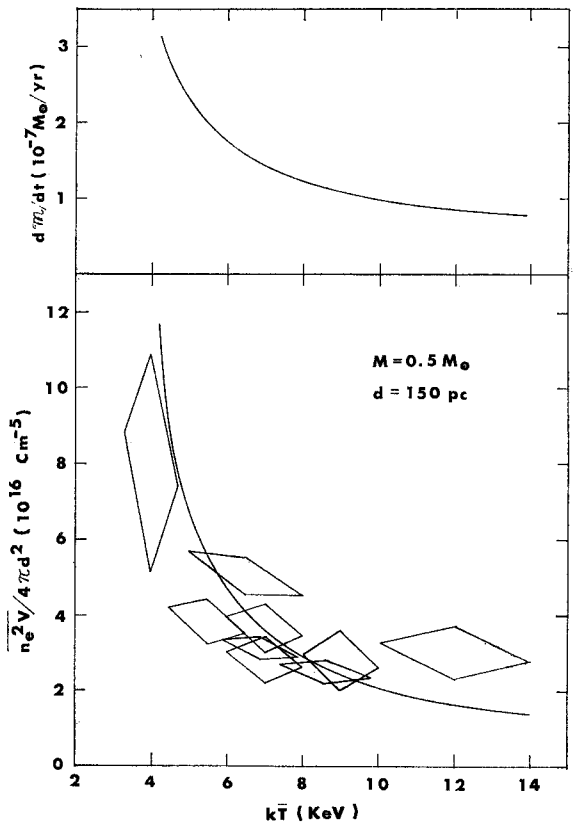

Fig. 2. Rocket observation of SCO X-1. The solid curve represents the result shown in Table II. The relation between the effective temperature and the accretion rate is shown in the upper diagram.

In a binary system just in the phase of mass exchange, it is natural to consider accreting material on to a secondary star to fluctuate with time. The mass exchange in a binary system is analogous to the overflow of water from a bath. The rate of overflow may be constant if the level surface of the bath is sufficiently quiet. It may change with time if the level surface is wavely perturbed. The surface of a primary star may also be perturbed with some respects such as pulsational and/or rotational instability. The spread of the observations in this diagram can be explained if the accretion rate fluctuates as much as a factor 3.

A question arises as to whether the approximation of stationary flow holds or not, when the accretion rate changes with time. As far as the emission region is concerned, the stationary approximation can be applicable when the time for a given infalling mass element to traverse the emission region, x/v, is much shorter than the time for an overall change of the density fluctuation of accreting material. The former time is estimated to be shorter than a second, while for the latter, although theoretical estimate is difficult at present, observational evidences show that it is longer than a minute even in a flickering stage of SCO X-1.[10]

As for the mean accretion rate, it is roughly related to the evolutionary time scale t_{ev} of a primary star as

$$\frac{d\mathcal{M}}{dt} \sim \frac{M_p}{t_{ev}}, \tag{25}$$

where M_p is the mass of the primary. A primary star larger than $5\,M_\odot$ can supply necessary accretion rate as in Fig. 2, even if the mass exchange occurs in the main-sequence stage of it. However, a possibility cannot be excluded that

a star less massive than $5\,M_\odot$, say even smaller than $2\,M_\odot$,[11] can also supply a necessary accretion, if the mass exchange commences in a subgiant or in a giant stage of the primary.

2) *B-magnitude*

Since the discovery of the optical counter part of SCO X-1, many simultaneous observations of optical magnitudes and X-ray intensities have been performed. In this subsection we will try to estimate the optical blue-magnitude B expected from the model. On account of relatively small thickness and low density, the emission region is almost transparent even for visible radiations. Visible radiations are mostly absorbed by widely spread and relatively cool accreting material outside the shock discontinuity. If the temperature of the accreting material is lower than that of the emission region, the energy emitted from the accreting material can be neglected as compared to that from the emission region. In this case, the accreting material plays only a role of a filter absorbing visible radiations.

Let the intensity of the free-free emission in the blue band be $F_{\rm ff}(B)$:

$$F_{\rm ff}(B)=\frac{h}{k\overline{T}}L_{\rm ff}e^{-h\nu_B/k\overline{T}}\frac{\bar{g}(B)}{\overline{G}}\frac{1}{4\pi d^2}\quad(\text{ergs/cm}^2\ \text{sec}\ \text{H}_\text{Z}),\tag{26}$$

where ν_B is the effective frequency for B-band, $\nu_B=6.84\times10^{14}\text{H}_\text{Z}$, and $\bar{g}(B)$ is the gaunt factor. Due to the absorption by accreting material, the intensity is reduced to

$$F(B)=F_{\rm ff}(B)e^{-\tau},\tag{27}$$

where the optical depth τ is approximated by[12]

$$\tau=\int_R^\infty\sqrt{3\kappa_{\rm e}\kappa_{\rm ff}}\,dr\,.\tag{28}$$

The free-free and the electron scattering opacities for visible frequency are written as

$$\begin{aligned}\kappa_{\rm ff}&=\kappa_{\rm ff_0}\rho^2T^{-3/2},\\ \kappa_{\rm e}&=\kappa_{\rm e_0}\rho\,,\end{aligned}\tag{29}$$

where $\kappa_{\rm ff_0}$ depends only on the frequency. The density in the absorption region can be calculated from the equation of continuity, Eq. (10), where the motion is assumed to follow Eq. (2),

$$\rho=\frac{1}{4\pi}\sqrt{\frac{1}{2GM}}\frac{1}{r^{3/2}}\frac{d\mathcal{M}}{dt}\,.\tag{30}$$

As for the temperature, it is difficult to estimate at present. Therefore, we define an averaged temperature $\overline{T}_{\rm env}$ for the absorption region, and in integration it is put outside the integrand. From Eqs. (28), (29) and (30), we have

$$\tau=\frac{4}{5}\sqrt{3\kappa_{\mathrm{ff}o}\kappa_{\mathrm{e}o}}\left\{\frac{1}{2(4\pi)^2GM}\left(\frac{d\mathcal{M}}{dt}\right)^2\right\}^{3/4}\frac{1}{\bar{T}_{\mathrm{env}}^{3/4}R^{5/4}}. \tag{31}$$

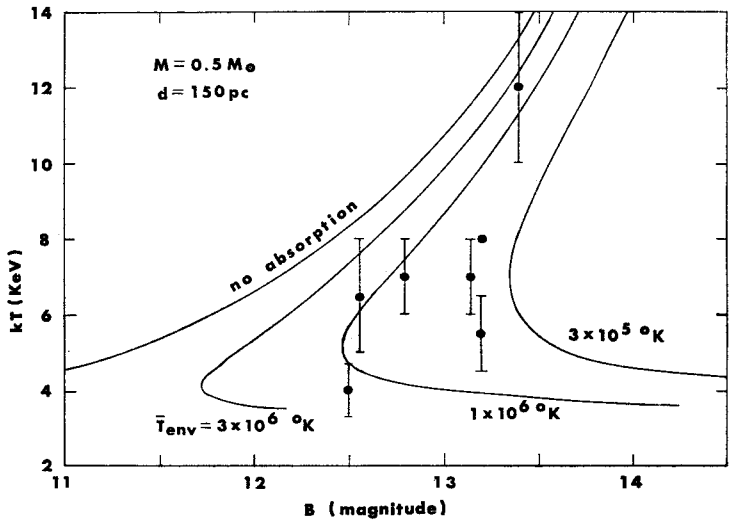

Fig. 3. The relation between the optical blue-magnitude B and the effective temperature of SCO X-1. Solid curves represents the result shown in Table III. A solid curve designated by no absorption shows the limiting case of no-absorption.

B-magnitude can be given in the term of $F(B)$ by

$$B=-2.5\log\frac{F(B)}{F(0)}, \tag{32}$$

where $F(0)$ is the intensity corresponding to $B=0$, which was calculated by Matthews and Sandage[18] as

$$F(0)=4.13\times10^{-20}\ \mathrm{ergs\ cm^{-2}\ sec^{-1}\ H_Z^{-1}}. \tag{33}$$

Table IV. The optical depth τ and the optical B-magnitude ($M=0.5M_\odot$, $d=150$ pc).

			$\bar{T}_{\mathrm{env}}=3\times10^6$ °K		$\bar{T}_{\mathrm{env}}=1\times10^6$ °K		$\bar{T}_{\mathrm{env}}=3\times10^5$ °K	
kT (KeV)	$\log F_{\mathrm{ff}}(B)$[a]	τ_{es}[b]	τ	B	τ	B	τ	B
3.56	−23.41	5.0	1.86	12.1	3.77	14.2	7.85	18.6
4.38	−23.75	2.8	0.76	11.7	1.56	12.6	3.24	14.4
5.47	−24.01	1.8	0.43	12.0	0.86	12.5	1.78	13.5
6.84	−24.22	1.4	0.27	12.4	0.55	12.7	1.15	13.3
8.21	−24.37	1.1	0.20	12.7	0.41	12.9	0.85	13.4
11.0	−24.60	0.9	0.14	13.2	0.28	13.3	0.58	13.7
13.7	−24.76	0.7	0.10	13.6	0.21	13.7	0.44	13.9

a) The unit on $F_{\mathrm{ff}}(B)$ is ergs/cm² sec Hz.
b) The optical depth of electron scattering is denoted by τ_{es}.

The optical thickness and B-magnitude are listed in Table IV for three cases, $\overline{T}_{\rm env}=3\times10^{5}$°K, 1×10^{6}°K and 3×10^{6}°K, respectively, where the distance d is also assumed to be 150 pc. Comparison to observations are made in the effective temperature-B-magnitude diagram (Fig. 3). Loci for constant $\overline{T}_{\rm env}$ are denoted by solid curves, while observations[1] are shown by black dots with error bars.

In low accretion phases, the B-magnitude decreases, that is, the X-ray source becomes brighter in the visible frequency range, as the accretion rate increases. When the accretion rate increases further, B-magnitude tends to increase, because the absorption overweighs the increase in the incident intensity $F_{\rm ff}(B)$. At some intense accretion phases, X-ray sources may become very faint.

It is to be noticed that the effect of interstellar absorption[14] is not taken into account in Table IV and in Fig. 3. This effect shifts the solid curves as a whole toward the high B-magnitude side. However, the solid curves are again shifted toward the left when the distance is assumed to be smaller than 150 pc.

3) *Hard X-rays*

In the previous section we have estimated the effective temperature in the emission region. This is considerably lower than that just behind the shock discontinuity (see Table I). In view of the above consideration the temperature may distribute in the emission region as shown schematically in Fig. 4. The excess emission of hard X-rays should be expected in the high-temperature region behind the shock front.

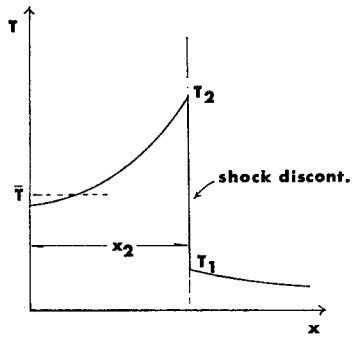

Fig. 4. Schematic diagram of the distribution of temperature in the emission region.

The intensity of emitted X-rays with energy $h\nu$ is given by

$$F_\nu=\frac{1}{4\pi d^2}\int_0^{x_2}\frac{1}{2}\frac{\varepsilon_{\rm ff}h}{kT}e^{-h\nu/kT}4\pi R^2\rho dx\,, \quad (34)$$

where $\varepsilon_{\rm ff}$ has been given in Eq. (15), and the factor 1/2 comes from the high-energy limit of the ratio of the gaunt factors[9] $\bar{g}/\bar{G}$. Suppose that in the high-temperature region we are interested in, the distribution of temperature is mainly determined from the cooling due to the free-free emission. Accordingly Eq. (12) can be approximated by

$$\frac{dT}{dx}=(\gamma-1)\frac{\mu H}{k}\frac{\varepsilon_{\rm ff}}{v}\,. \quad (35)$$

In term of this equation, Eq. (34) can be written as

$$F_\nu=\frac{1}{8\pi d^2}\frac{1}{\gamma-1}\frac{h}{\mu H}\frac{d\mathcal{M}}{dt}\int_{y_2}^{\bar{y}}\left(\frac{e^{-y}}{y}\right)dy\,, \quad (36)$$

where

$$y = h\nu/kT\,. \tag{37}$$

Results are shown in Table V for two cases with $M=0.5\,M_\odot$, $\log \overline{T}=7.71$ and $M=0.6\,M_\odot$, $\log \overline{T}=7.74$; corresponding physical values have been shown in the fourth row of Tables II(a) and II(b), respectively. The distance is also assumed to be 150 pc for the both cases. In Fig. 5 results of Table V are illustrated together with the intensities corresponding to the respective effective temperatures.

Table V. The intensities of hard X-rays ($d=150$ pc).

	$M=0.5M_\odot$ $\log \overline{T}=7.71$	$M=0.6M_\odot$ $\log \overline{T}=7.74$
$h\nu$ (KeV)	$\log F_\nu$[a)]	$\log F_\nu$
100	−2.80	−1.59
70	−1.86	−0.90
50	−1.12	−0.37
30	−0.51	−0.02

a) The unit on F_ν is KeV/KeV cm² sec.

It is to be noticed that the intensity of hard X-ray is proportional to the accretion rate $d\mathcal{M}/dt$. Therefore, we can expect a correlation between the intensity of hard X-ray and the effective temperature, that is, intense hard X-rays are expected in phases of low effective temperature.

Comparison to observations are made in Fig. 6 for the case of $0.5\,M_\odot$ star.

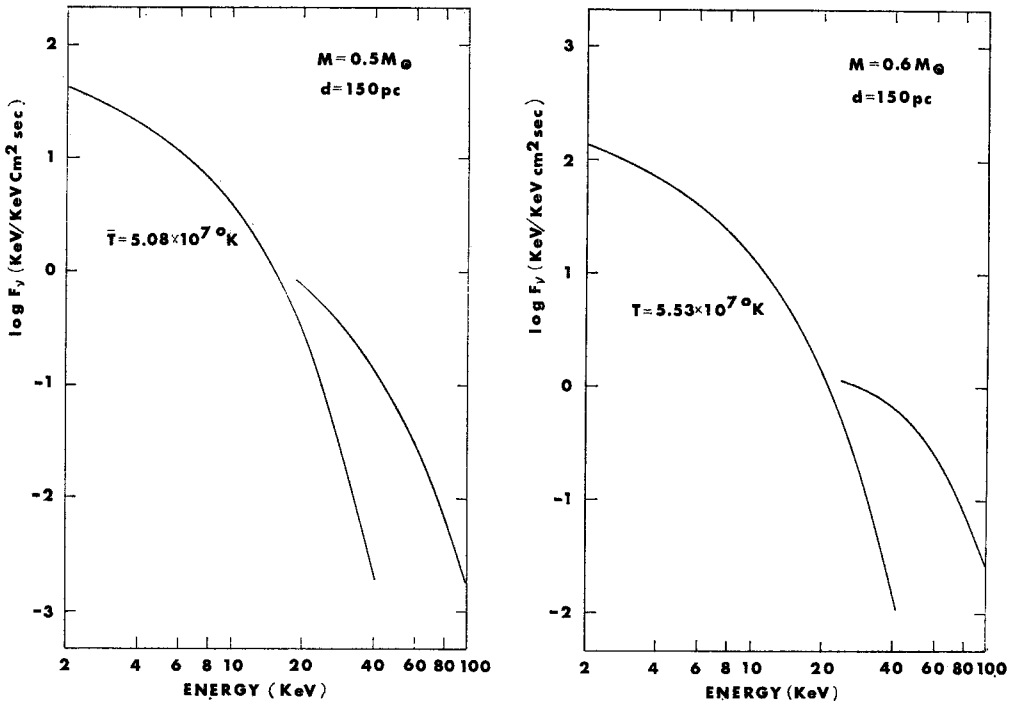

Fig. 5. The energy spectra of X-rays from white dwarfs of $0.5M_\odot$ and $0.6M_\odot$ for particular phases selected so as to give the effective temperature $\overline{T}\sim 5\times 10^7$°K.

The calculated intensity corresponds to rather high accretion phase as is seen from Fig. 2. In low accretion phases the intensities become as lower as about a factor 3. The observational values are taken after Agarwal et al.[15]

§ 5. Discussion

In the previous section we have chosen a white dwarf of mass $0.5\,M_\odot$. One of the reason for this choice is that the lower limit of the temperature in high-accretion limit (see Fig. 2) coincides with the observed values of SCO X-1. However, this lower limit T_l is related to the mean velocity v as $T_l=\mu Hv^2/k$, as is obtained from Eq. (18). Recently, Aizu[16] has shown that the emission region can be solved analytically in high-accretion limit. According to his result the mean velocity can be approximated by $v^2\sim v_2^2/4$ instead of Eq. (23). This means that the mass of a white dwarf may be $0.7\sim1\,M_\odot$ in order to explain the observed nature of SCO X-1.

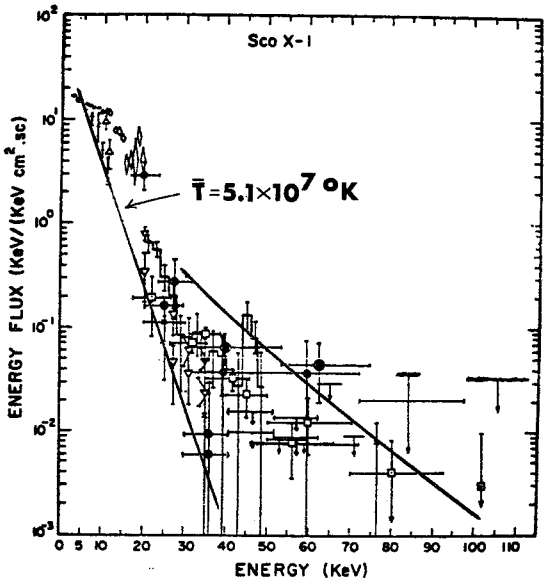

Fig. 6. X-ray intensities of SCO X-1 (after Agarwal et al.[15]), together with the predicted X-ray intensity from $0.5M_\odot$ white dwarf.

In this paper the emission region is characterized by a mean effective temperature. However, in real cases the distribution of the temperature in the emission region may not be so simple as represented by an effective temperature. The corresponding energy spectrum may also deviate from that illustrated in Fig. 5. Furthermore, a half of emitted X-rays are radiated on the average toward the inner direction. These radiations should be absorbed by optically thick-inner region, and re-emitted again. Then, more critical treatments are necessary for further details of the model, even if the emission region is transparent for the emitted radiation.

Acknowledgements

The author wishes to express many thanks to Professor K. Aizu for his encouragement and critical comments. He also wishes to express his thanks to Dr. M. Matsuoka and Dr. H. Yokoo for stimulating discussions.

References

1) T. Kitamura, M. Matsuoka, S. Miyamoto, M. Nakagawa, M. Oda, Y. Ogawara, K. Takagishi, U. R. Rao, E. V. Chitnis, U. B. Jayanthi, A. S. Prakasa-Rao and S. M. Bhandari, Astrophys. Space Sci. **12** (1971), 378.
2) E. Schreier, R. Levinson, H. Gursky, E. Kellogg, H. Tananbaum and R. Giacconi, Astrophys. J. **172** (1972), L79.
3) R. E. Wilson, Astrophys. J. **174** (1972), L27.
Y. Osaki, Publ. Astron. Soc. Japan **24** (1972), 419.
4) S. Sakashita, Prog. Theor. Phys. **39** (1968), 235.
5) W. H. McCrea, Astrophys. J. **124** (1956), 461.
6) L. D. Landau and E. M. Lifshitz, *Fluid Mechanics* (Pergamon Press, London, 1959).
7) S. Chandrasekhar, *An Introduction to the Study of Stellar Structure* (Dover Pub. INC., New York, 1957).
8) S. Hayakawa, M. Matsuoka and D. Sugimoto, Space Sci. Rev. **5** (1966), 109.
9) G. Bekefi, *Radiation Process in Plasmas* (Hohn Wiley and Sons, INC., New York, 1966).
10) M. Matsuoka, M. Fujii, S. Miyamoto, J. Nishimura, M. Oda, Y. Ogawa, S. Hayakawa, I. Kasahara, F. Makino and Y. Tanaka, a preprint (1972).
11) R. Kippenhahn, K. Kohl and A. Weigert, Z. Astrophys. **66** (1967), 58.
12) W. H. Tucker, Astrophys. J. **149** (1967), L105.
13) T. A. Matthews and A. R. Sandage, Astrophys. J. **138** (1963), 30.
14) G. Neugebauer, J. B. Oke, E. Becklin and G. Garmire, Astrophys. J. **155** (1969), 1.
15) P. C. Agarwal, S. Biswas, G. S. Gokhale, V. S. Iyengar, P. K. Kunte, R. K. Manchanda and B. V. Sreekantan, *Non-Solar X- and Gamma-Ray Astronomy* (D. Reidel Pub. Co., Dodrecht-Holland, 1970).
16) K. Aizu, private communication (1972).